Letter Vol. 45, No. 6 / 15 March 2020 / Optics Letters 1415

Topological photonic crystal fibers and ring resonators

Laura Pilozzi,[1,*] Daniel Leykam,[2] Zhigang Chen,[3,4] and Claudio Conti[1,5]

[1]Institute for Complex Systems, National Research Council (ISC-CNR), Via dei Taurini 19, 00185 Rome, Italy
[2]Center for Theoretical Physics of Complex Systems, Institute for Basic Science (IBS), Daejeon 34126, South Korea
[3]The Key Laboratory of Weak-Light Nonlinear Photonics, TEDA Applied Physics Institute, Nankai University, Tianjin 300457, China
[4]Department of Physics and Astronomy, San Francisco State University, San Francisco, California 94132, USA
[5]Department of Physics, University Sapienza, Piazzale Aldo Moro 5, 00185 Rome, Italy
*Corresponding author: laura.pilozzi@isc.cnr.it

Received 30 December 2019; revised 6 February 2020; accepted 9 February 2020; posted 10 February 2020 (Doc. ID 387043); published 5 March 2020

With an exact recursive approach, we study photonic crystal fibers and resonators with topological features induced by Aubry–Andre–Harper cladding modulation. We find nontrivial gaps and edge states at the interface between regions with different topological invariants. These structures show topological protection against symmetry-preserving local perturbations that do not close the gap and sustain strong field localization and energy concentration at a given radial distance. As topological light guiding and trapping devices, they may bring about many opportunities for both fundamentals and applications unachievable with conventional devices.

https://doi.org/10.1364/OL.387043

The seminal papers on analogs of quantum Hall effect in optics [1,2] boosted the research on photonic topological insulators, described by magnetic-like Hamiltonians [3–7]. They hold great promises for applications such as topological lasers [8–11], protected frequency combs [12], and topological nanostructures [13,14] for quantum information processing [15–17]. Edge states lying in the bulk gaps are the leading ingredient in these applications. Localized at the boundary between regions with diverse topological invariants [18] as the first Chern number of the bands—or the winding number of the gaps [19]—they are robust against backscattering from impurities. Recent developments rely on machine learning techniques to design topological structures [20,21]. A possible way to get nontrivial photonic topological phases is to employ synthetic dimensions [22–25]. An example is Aubry–Andre–Harper (AAH) modulation [26–28] of optical lattice parameters. One-dimensional (1D) systems with synthetic dimensions have the same topological features as their 2D periodic ancestor lattices [29,30]. However, the application of synthetic dimensions has so far been limited to linear geometries. The use of AAH and similar strategies for synthetic dimensions in circular, elliptical, or more complex coordinates is unexplored. In this Letter, we introduce the concept of topological photonic crystal fibers (PCFs) and resonators that exploit topological features due to AAH modulation in cylindrical symmetry to guide and trap electromagnetic radiation on edge states. These new optical devices support tightly confined modes in the radial direction, protected with respect to radial disorder. Conventional waveguides and resonators exploit either total internal reflection (TIR), with a solid core surrounded by a lower refractive index medium, or photonic crystal claddings [31–33] to guide light in a hollow core by Bragg reflection. Advanced PCFs enable control of the angular momentum [34], induce optomechanical nonlinearities [35], and may guide dielectric particles by radiation pressure [36]. The photonic bandgap mechanism allows annular Bragg resonators [37]. Reconfigurable index structures are designed by Bessel photonic lattices in bulk crystals [38], as well as one-way fiber modes at microwave frequencies [39], backscattering immune, in a 3D magnetic Weyl photonic crystal. Our proposal of a cylindrical topological insulator, sustaining edge states, is a recipe for the cladding of PCFs to obtain strongly localized fields, topologically protected. Indeed, in our configuration, the core–cladding interface acts as the boundary between two distinct topological phases: a trivial one, the core, and a topological one, the cladding with radiative edge states [30]. This boundary can also be attained inside the cladding if a radial distance ρ_n value divides it into two substructures with different modulations.

The structure considered has a core of dielectric constant ϵ_c and radius ρ_1 and a cladding given by a sequence of two homogeneous layers A and B characterized by dielectric functions ϵ_a and ϵ_b. The center positions of the A layers, s_a wide, are given by $\rho_n^A = d_o[n + \eta\delta_n^H]$, where $\delta_n^H = \cos(2\pi\gamma n + \phi)$ is Harper modulation [26], with $\gamma = p/q$, and p and q are coprime integer numbers [29]; η controls the modulation strength. The cladding, in the ρ direction, is a periodic structure of period $d = qd_o$, where d_o is the period of the unmodulated structure ($\eta = 0$). The phase ϕ, the topological parameter, varying in $(0, 2\pi)$, adiabatically deforms the system and accounts for the momentum along the second geometrical dimension of the 2D ancestor lattice [30]. The mapping 1D → 2D allows introducing the topological indices. The 2D system shows a broken time inversion symmetry that can be interpreted as the presence of an

effective or "synthetic" magnetic field. This imposes conditions on the unit cell of the structure that must lack an inversion center in order to have nontrivial topological invariants and edge states. This requires at least three-layer A in the unit cell, and a minimal model would have $p=1$ and $q=3$. For this annular regions sequence, the interface positions are $\rho_j=\rho_j'+\delta$, where $\rho_j'=\rho^A_{\lfloor\frac{j+1}{2}\rfloor}+(-1)^{j-2\lfloor\frac{j-1}{2}\rfloor}s_a/2$, $\delta=\rho_1-\rho_1'$, and $\lfloor x\rfloor$ is the integer part of x. Different methods for the analysis of structured claddings have been proposed in the literature, ranging from approximated ones such as the method using asymptotic approximations of Bessel functions [40], to exact ones such as the standard transfer matrix method [31]. We apply an exact recursive approach [41] to analyze the bandgap structure and design the resonator, since casting the problem in a 2×2 matrix form for the longitudinal components of the electric and magnetic fields allows to obtain, in a straightforward way, the complex mode frequencies. This recursive formalism enables us to find the modal distribution in the case of an arbitrary arrangement of annular concentric regions and so to study the effects of shallow disorder and verify the topological protection. Figure 1 schematically illustrates (a) the topological PCF, (b) the topological optical resonator, and (c) their radial index profile. In these systems, the permittivity depends only on the radial coordinate: $\epsilon(\rho)=\epsilon_j$ for $\rho_{j-1}<\rho<\rho_j$, with $\rho_0=0$. In cylindrical coordinates, for waves traveling in the z direction with propagation constant β, every field component has the form $\psi(\rho,\vartheta,z,t)=\psi(\rho,\vartheta)e^{i(\beta z-\omega t)}$, where ω is the angular frequency. In each homogeneous cylindrical layer, the longitudinal field components $E_z^j(\rho,\vartheta)$ and $H_z^j(\rho,\vartheta)$ are the solutions to $[\frac{\partial^2}{\partial\rho^2}+\frac{1}{\rho}\frac{\partial}{\partial\rho}+(k_j^2-\frac{\ell^2}{\rho^2})]X_z^j(\rho,\vartheta)=0$, where $X=E$, H, l is an integer representing the angular modal number, and $k_j^2=\frac{\omega^2}{c^2}\epsilon_j-\beta^2$, with c the speed of light. We choose, as independent solutions, the Bessel $J_\ell(k_j\rho)$ and Hankel $H_\ell^{(1)}(k_j\rho)$ functions of the first kind so that inside each homogeneous cylindrical layer j, the field can be written as the superposition of an outgoing wave $H_\ell^{(1)}(k_j\rho)$ and a standing wave $J_\ell(k_j\rho)$ [41]: $[E_z^j,\,H_z^j]^T=[H_\ell^{(1)}(k_j\rho)\overleftrightarrow{I}+J_\ell(k_j\rho)\overleftrightarrow{\tilde{R}}_{j,j+1}]\vec{a}_j$. Here $\vec{a}_j\equiv[e_{jz},\,h_{jz}]^T$ determines the relative amplitudes of the electric and magnetic field components, and $\overleftrightarrow{\tilde{R}}_{j,j+1}$, giving the relation between the electric and magnetic field components of the inward and outward propagating fields, is a generalized reflection matrix. Recursive relations can be obtained for both the reflection matrices and the field amplitudes [41].

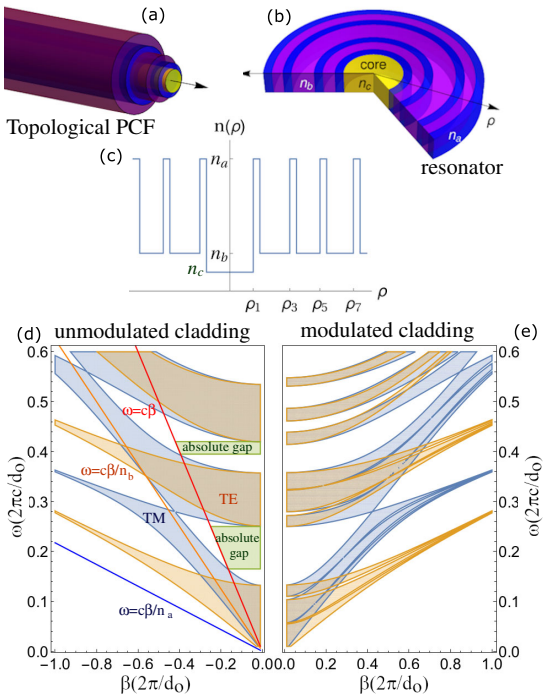

Fig. 1. (a) Topological PCF, (b) optical resonator, and (c) dielectric function profile for a cladding with $\gamma=1/3$, taking on the values n_c for the core, and n_a, n_b for the cladding. Asymptotic bands for (d) unmodulated and (e) modulated cladding with $\phi=\pi/6$, $\eta=0.2/\pi$, $n_a=4.6$ (tellurium), $n_b=1.6$ (polystyrene), $s_a=0.33d_o$, and $s_b=0.67d_o$; $n_c=1$. Filled regions are TE (orange) and TM (blue) propagating modes.

The generalized reflection matrix, $\overleftrightarrow{\tilde{R}}_{j,j+1}$, includes the effects of reflections and transmissions at all the layers beyond the j-th one. With this equation and starting from the outermost, one can find the reflection and transmission matrices for all the N layers; then, starting from the innermost layer, the field can be recursively described in the whole structure. The boundary conditions for the fields at $\rho=\rho_j$ determine the reflection and transmission matrices $\overleftrightarrow{R}_{j,j+1}$ and $\overleftrightarrow{T}_{j,j+1}$. Guided modes, defined as the nontrivial solutions that exist without the need for an external excitation, can be found requiring that the reflection matrix have an infinite determinant. The guidance condition, given for a two-layer structure in [42], for an N-layer fiber can be obtained from the generalized reflection matrix, and reads $\det(\overleftrightarrow{I}-\overleftrightarrow{R}_{2,1}\overleftrightarrow{\tilde{R}}_{2,3})\equiv f(\omega,\beta)=0$. Its solutions, giving rise to a set of complex (ω,β) states with either real frequency or real wave vector, are the allowed modes of the fiber. Unlike Bragg guiding fibers, the core–cladding interface acts as the boundary between two distinct topological phases: a trivial core and a topological cladding with radiative edge states [30], here described in the complex ω representation [43], where the real part is the modal resonance frequency while the imaginary part is the decay rate accounting for the loss [44]. This description is equivalent [45] to the one with real frequency and complex propagation constant β, with the imaginary part of β providing the radiative decay of the leaky modes [31,46].

Due to the radial periodic cladding structuring, our topological PCF shows a gapped spectrum. It cannot be analyzed in the framework of the Bloch theorem since, for radially depending dielectric functions, the operator $-\frac{1}{\rho\epsilon(\rho)}\frac{\partial}{\partial\rho}\frac{\rho}{\mu(\rho)}\frac{\partial}{\partial\rho}+\frac{\ell^2}{\rho^2\epsilon(\rho)\mu(\rho)}$ is not invariant under translations. However, as detailed in Ref. [42], one can always identify a ρ_n value such that for $\rho>\rho_n$, the structure shows gaps converging to that of a planar structure with the same Harper modulation.

For a cladding consisting of alternating layers of n_a and n_b refractive indices, Figs. 1(d) and 1(e) show the one-dimensional gaps and bands in the asymptotic limit: (d) is the case of a periodic unmodulated cladding, while (e) includes the modulation. This modulation adds additional gaps where we expect to find guided modes as well as edge states; the gap dependence

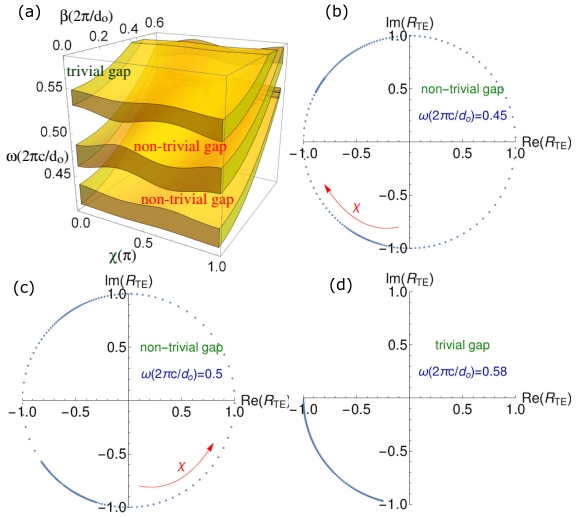

Fig. 2. (a) TE asymptotic bands for a modulated cladding as a function of χ and β. Phase of the reflection coefficient for the three gaps for which the winding numbers w are: (b) -1, (c) 1, and (d) 0.

on the shifted phase $\chi = \phi - \frac{\pi}{6}$ is shown in Fig. 2(a) for TE polarization, in the dimensionless energy range (0.41,0.58). Both plots in Figs. 1 and 2 are obtained through the quantity $2\xi = -\mathrm{Tr}[T(\omega, \beta, \chi)]$, involving the trace of the transfer matrix $T(\omega, \beta, \chi)$ in the asymptotic limit, allowing one to locate the cladding gaps in the regions where $\xi^2 > 2$. To take into account the finite value of the core radius ρ_1, affecting the actual position of the allowed modes, gaps ($|\tilde{\mathbf{R}}_{1,2}|^2 = 1$) and bands ($|\tilde{\mathbf{R}}_{1,2}|^2 < 1$) of the system can be equally well located through the reflectivity modulus map $|\tilde{\mathbf{R}}_{1,2}(\omega, \beta, \chi)|^2$. The generalized reflectivity at the core–cladding interface also allows to define the nature of the gaps [43]. In Figs. 2(b)–2(d), we show, for the three different gaps of Fig. 2(a), the winding numbers w_i of the reflection coefficient, i.e., the reflectivity extra phase acquired when χ varies in the range $(-\pi, \pi)$ while ω remains inside the gap. A nonzero winding number corresponds to a topologically nontrivial sample and is tied to the existence of topological edge states [47–49]. So, unlike the upper one, the two lower gaps are nontrivial. Moreover, through the reflectivity poles, edge state dispersions can be calculated. The one in the lower gap is shown in Fig. 3(a) as a blue curve, bridging the gap in a given (χ, β) range. Figs. 3(b) and 3(c) show the TE reflectivity map in the plane [$(\mathrm{Re}(\omega), \chi)$ (b) and $(\mathrm{Re}(\omega), \beta)$ (c)] for a structure with the same parameters as Fig. 2 but a finite core radius $\rho_1 = 2d_o$. In this figure, topological edge states are clearly seen: their real part $\mathrm{Re}(\omega)$ is shown as a dotted curve, while $\mathrm{Im}(\omega) \approx 10^{-2}\mathrm{Re}(\omega)$. We notice that, as they live in the gap's spectrum, edge states cannot be removed or added unless a topological transition of the bulk bands happens when the gap closes. This gives them a topological protection against radial disorder. We verify this hallmark property by introducing a randomized perturbation of the A layers' center positions. In this case, $\rho_n^A = d_o(n + \eta(\delta_n^H + \sigma\xi_n))$, where ξ_n are random variables chosen in the range $(-1, 1)$, while σ is the disorder strength. Figure 3(d) shows the frequency variation of a specific mode for two realizations of increasing random disorder; it proves that it is nearly unaffected, even for large perturbations ($\sigma \simeq 0.5$). The different behavior for the two realizations is due mainly to the lattice pitch variation with disorder: for the orange (blue) curve, the lattice pitch increases (decreases). As a consequence, the whole spectrum shifts to higher (lower) energies for decreasing (increasing) pitch. Curves for different core radius values show unnoticeable differences since the mode frequencies depend mainly on the cladding features. The topological PCF preserves the time-inversion symmetry, so in the z direction, light guiding is not unidirectional. However, within the literature on topological waveguides, backscattering in the z direction can be safely neglected due to the absence of strong scatterers capable of inducing such a large momentum change. In our case, what is important is the robustness to radial perturbations and imperfections, which are the main source of the (low) losses in PCFs. Such losses accumulate slowly during propagation along the fiber due to disorder-induced coupling between the core and cladding exterior, which our novel design addresses.

With respect to the modulation phase, the dispersion relations are anyway nonreciprocal with the positive/negative χ values corresponding to states localized at the left or right boundary of the cladding. Finally, the normalized E-field pattern, Fig. 4, confirms the strong localization at the core–cladding interface, unlike TIR or bandgap fibers. This localization of the edge mode shields the cladding from the absorption of guided light.

In the study of band structures in a cylindrical geometry with AAH modulation of the refractive index, we demonstrate, through an exact recursive approach, the existence of edge modes with topological dispersion in the gapped spectrum, robust to disorder and strongly localized in the radial direction. While there is no "synthetic interface" in our system, the phase χ plays a special role because it parameterizes a topologically nontrivial family of fiber designs. Namely, as χ is varied, the nontrivial topological invariants of the family guarantee an edge state will be pumped through the bulk band gap. Importantly, this means there is an optimal χ hosting a mid-gap mode with

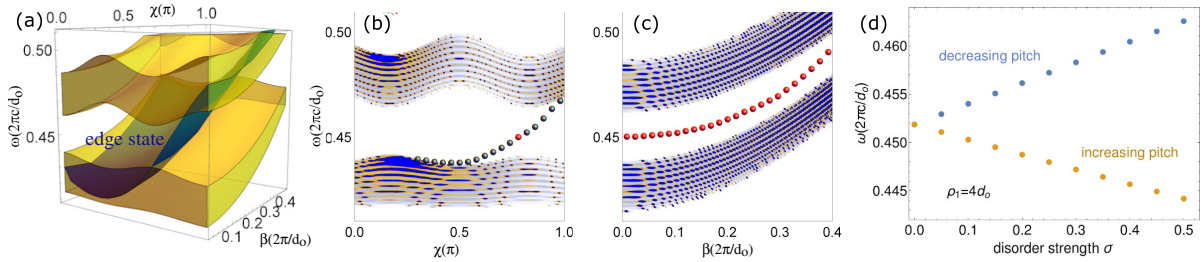

Fig. 3. TE reflectivity map and edge states (a) in the asymptotic limit and the exact solution for (b) $\beta = 0.1(2\pi/d_o)$ and (c) $\chi = 0.8\pi$. (b), (c) Finite cladding with 13 unit cells. (d) Edge mode for $\beta = 0.1(2\pi/d_o)$ and $\chi = 0.8\pi$ as a function of the disorder strength for two realizations: the orange (blue) curve is for a system with an increasing (decreasing) normalized period, d/d_o.

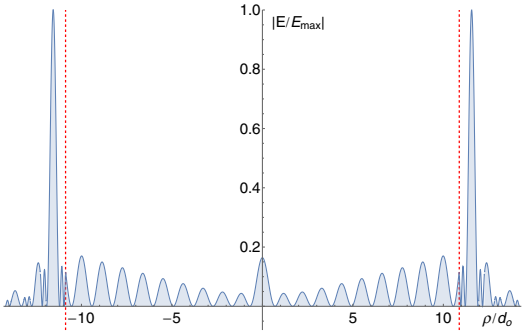

Fig. 4. TE, $\ell = 0$, edge mode normalized field profile for $\chi = 0.8\pi$, $\beta = 0.1(2\pi/d_o)$, and $\omega(2\pi c/d_o) = 0.452 + 0.6 * 10^{-2} i$. Dashed red lines mark the core region boundaries.

strongest localization and therefore minimizing losses due to effects such as surface roughness of the cladding. Thus, the topology of the synthetic dimension can be used to systematically determine which families of fiber designs can support optimally localized cladding modes. Optical fibers with topologically protected states open many new perspectives in the transmission of information for classical and quantum applications. The resilience to external perturbations enables low-loss transport, quantum transport of non-classical states, and low-threshold topological fiber lasers. Future directions also include the study of topological eigenmodes with angular momentum for multilevel signals, the study of the interplay between the Berry phase in twisted fibers and Chern numbers in synthetic dimensions, topological ring resonators for frequency comb generation, and linear and nonlinear metasurfaces by single and coupled resonators with radial Harper modulations. Hollow-core fibers can accelerate dielectric and metallic particles; the way topological physics alters radiation pressure and related phenomena—as optomechanical nonlinearities—is a new research direction. We envisage many new physical phenomena when considering multimodal optical fibers with topologically protected states.

Funding. Horizon 2020 Framework Programme (820392, 731473); Ministero dell'Istruzione, dell'Università e della Ricerca (20177PSCKT, 2015KEZNYM); National Key Research and Development Program of China (017YFA0303800); Institute for Basic Science, Korea (IBS-R024-Y1).

Disclosures. The authors declare no conflicts of interest.

REFERENCES

1. S. Raghu and F. D. M. Haldane, Phys. Rev. A **78**, 033834 (2008).
2. F. D. M. Haldane and S. Raghu, Phys. Rev. Lett. **100**, 013904 (2008).
3. Z. Wang, Y. Chong, J. D. Joannopoulos, and M. Soljačić, Nature **461**, 772 (2009).
4. M. Hafezi, E. A. Demler, J. M. Lukin, and M. D. Taylor, Nat. Phys. **7**, 907 (2011).
5. K. Fang, Z. Yu, and S. Fan, Nat. Photonics **6**, 782 (2012).
6. M. Hafezi, S. Mittal, J. Fan, A. Migdall, and J. M. Taylor, Nat. Photonics **7**, 1001 (2013).
7. S. Longhi, Phys. Rev. Lett. **122**, 237601 (2019).
8. L. Pilozzi and C. Conti, Phys. Rev. B **93**, 195317 (2016).
9. P. St-Jean, V. Goblot, E. Galopin, A. Lemaître, T. Ozawa, L. Le Gratiet, I. Sagnes, J. Bloch, and A. Amo, Nat. Photonics **11**, 651 (2017).
10. G. Harari, M. A. Bandres, Y. Lumer, M. C. Rechtsman, Y. D. Chong, M. Khajavikhan, D. N. Christodoulides, and M. Segev, Science **359**, eaar4003 (2018).
11. B. Bahari, A. Ndao, F. Vallini, A. El Amili, Y. Fainman, and B. Kanté, Science **358**, 636 (2017).
12. L. Pilozzi and C. Conti, Opt. Lett. **42**, 5174 (2017).
13. S. Kruk, A. Poddubny, D. Smirnova, L. Wang, A. Slobozhanyuk, A. Shorokhov, I. Kravchenko, B. Luther-Davies, and Y. Kivshar, Nat. Nanotechnol. **14**, 126 (2019).
14. K. Koshelev, G. Favraud, A. Bogdanov, Y. Kivshar, and A. Fratalocchi, Nanophotonics **8**, 725 (2019).
15. S. Mittal, V. V. Orre, and M. Hafezi, Opt. Express **24**, 15631 (2016).
16. M. C. Rechtsman, Y. Lumer, Y. Plotnik, A. Perez-Leija, A. Szameit, and M. Segev, Optica **3**, 925 (2016).
17. S. Mittal, E. A. Goldschmidt, and M. Hafezi, Nature **561**, 502 (2018).
18. D. J. Thouless, M. Kohmoto, M. P. Nightingale, and M. den Nijs, Phys. Rev. Lett. **49**, 405 (1982).
19. Y. Hatsugai, Phys. Rev. B **48**, 11851 (1993).
20. L. Pilozzi, F. A. Farrelly, G. Marcucci, and C. Conti, Commun. Phys. **1**, 57 (2018).
21. Y. Long, J. Ren, Y. Li, and H. Chen, Appl. Phys. Lett. **114**, 181105 (2019).
22. T. Ozawa, H. M. Price, N. Goldman, O. Zilberberg, and I. Carusotto, Phys. Rev. A **93**, 043827 (2016).
23. L. Yuan, Q. Lin, M. Xiao, and S. Fan, Optica **5**, 1396 (2018).
24. E. Lustig, S. Weimann, Y. Plotnik, Y. Lumer, M. A. Bandres, A. Szameit, and M. Segev, Nature **567**, 356 (2019).
25. A. Dutt, Q. Lin, L. Yuan, M. Minkov, M. Xiao, and S. Fan, Science **367**, 59 (2020).
26. P. G. Harper, Proc. Phys. Soc. A **68**, 879 (1955).
27. S. Aubry and G. André, Ann. Israel Phys. Soc. **3**, 18 (1980).
28. S. Ganeshan, K. Sun, and S. Das Sarma, Phys. Rev. Lett. **110**, 180403 (2013).
29. D. R. Hofstadter, Phys. Rev. B **14**, 2239 (1976).
30. A. V. Poshakinskiy, A. N. Poddubny, L. Pilozzi, and E. L. Ivchenko, Phys. Rev. Lett. **112**, 107403 (2014).
31. P. Yeh, A. Yariv, and E. Marom, J. Opt. Soc. Am. **68**, 1196 (1978).
32. P. St.J. Russell, Science **299**, 358 (2003).
33. J. C. Knight, J. Broeng, T. A. Birks, and P. St.J. Russell, Science **282**, 1476 (1998).
34. G. K. L. Wong, M. S. Kang, H. W. Lee, F. Biancalana, C. Conti, T. Weiss, and P. St.J. Russell, Science **337**, 446 (2012).
35. A. Butsch, C. Conti, F. Biancalana, and P. St.J. Russell, Phys. Rev. Lett. **108**, 093903 (2012).
36. M. K. Garbos, T. G. Euser, O. A. Schmidt, S. Unterkofler, and P. St.J. Russell, Opt. Lett. **36**, 2020 (2011).
37. J. Scheuer and A. Yariv, J. Opt. Soc. Am. B **20**, 2285 (2003).
38. X. Wang, Z. Chen, and J. Yang, Opt. Lett. **31**, 1887 (2006).
39. L. Lu, H. Gao, and Z. Wang, Nat. Commun. **9**, 5384 (2018).
40. Y. Xu, R. K. Lee, and A. Yariv, Opt. Lett. **25**, 1756 (2000).
41. W. C. Chew, *Waves and Fields in Inhomogeneous Media* (Van Nostrand Reinhold, 1990).
42. L. Pilozzi, D. Leykam, Z. Chen, and C. Conti, arXiv:1909.02081 (2019).
43. A. V. Poshakinskiy, A. N. Poddubny, and M. Hafezi, Phys. Rev. A **91**, 043830 (2015).
44. Y. Xu, W. Liang, A. Yariv, J. G. Fleming, and S.-Y. Lin, Opt. Lett. **28**, 2144 (2003).
45. K. C. Huang, E. Lidorikis, X. Jiang, J. D. Joannopoulos, K. A. Nelson, P. Bienstman, and S. Fan, Phys. Rev. B **69**, 195111 (2004).
46. S. G. Johnson, M. Ibanescu, M. Skorobogatiy, O. Weisberg, T. D. Engeness, M. Soljačić, S. A. Jacobs, J. D. Joannopoulos, and Y. Fink, Opt. Express **9**, 748 (2001).
47. M. Hafezi, Phys. Rev. Lett. **112**, 210405 (2014).
48. S. Mittal, S. Ganeshan, J. Fan, A. Vaezi, and M. Hafezi, Nat. Photonics **10**, 180 (2016).
49. M. Atala, M. Aidelsburger, J. T. Barreiro, D. Abanin, T. Kitagawa, E. Demler, and I. Bloch, Nat. Phys. **9**, 795 (2013).